ORIGINAL ARTICLE

JBMR®

CCL20/CCR6 Signaling Regulates Bone Mass Accrual in Mice

Michele Doucet, Swaathi Jayaraman, Emily Swenson, Brittany Tusing, Kristy L Weber,* and Scott L Kominsky

Department of Orthopaedic Surgery, Johns Hopkins University School of Medicine, Baltimore, MD, USA

ABSTRACT

CCL20 is a member of the macrophage inflammatory protein family and is reported to signal monogamously through the receptor CCR6. Although studies have identified the genomic locations of both *Ccl20* and *Ccr6* as regions important for bone quality, the role of CCL20/CCR6 signaling in regulating bone mass is unknown. By micro–computed tomography (μCT) and histomorphometric analysis, we show that global loss of *Ccr6* in mice significantly decreases trabecular bone mass coincident with reduced osteoblast numbers. Notably, CCL20 and CCR6 were co-expressed in osteoblast progenitors and levels increased during osteoblast differentiation, indicating the potential of CCL20/CCR6 signaling to influence osteoblasts through both autocrine and paracrine actions. With respect to autocrine effects, CCR6 was found to act as a functional G protein–coupled receptor in osteoblasts and although its loss did not appear to affect the number or proliferation rate of osteoblast progenitors, differentiation was significantly inhibited as evidenced by delays in osteoblast marker gene expression, alkaline phosphatase activity, and mineralization. In addition, CCL20 promoted osteoblast survival concordant with activation of the PI3K-AKT pathway. Beyond these potential autocrine effects, osteoblast-derived CCL20 stimulated the recruitment of macrophages and T cells, known facilitators of osteoblast differentiation and survival. Finally, we generated mice harboring a global deletion of *Ccl20* and found that *Ccl20*$^{-/-}$ mice exhibit a reduction in bone mass similar to that observed in *Ccr6*$^{-/-}$ mice, confirming that this phenomenon is regulated by CCL20 rather than alternate CCR6 ligands. Collectively, these data indicate that CCL20/CCR6 signaling may play an important role in regulating bone mass accrual, potentially by modulating osteoblast maturation, survival, and the recruitment of osteoblast-supporting cells. © 2016 American Society for Bone and Mineral Research.

KEY WORDS: OSTEOBLAST; BONE MODELING AND REMODELING; CELL/TISSUE SIGNALING; CYTOKINES

Introduction

CCL20 (MIP-3α) is a member of the macrophage inflammatory protein (MIP) family, which was discovered in 1988 and consists of six chemokines of the CC type. Amongst CC chemokines, including those of the MIP family, CCL20 has some distinctive characteristics. Although most chemokines are promiscuous in their ligand-receptor interactions, CCL20 participates in a monogamous ligand-receptor relationship, wherein it signals through a single receptor, CCR6, which in turn serves solely as the receptor for CCL20.[1] Further, although showing conservation among species,[2,3] the gene structure of *Ccl20* differs from that of the CC chemokine family and is located in a genomic region apart from that in which most CC chemokine genes are clustered. Expression of CCL20 has been reported on epithelial surfaces of the liver, lung, and intestine, as well as in bone marrow and secondary lymphoid organs.[4] Evidence suggests that CCL20 functions in both homeostatic and inflammatory capacities, regulating the residence of leukocytes at specific organ sites and the recruitment of immune cells (eg, dendritic cells, T cells, B cells) in response to inflammatory signals, respectively.[5–7] Indeed, *Ccr6*$^{-/-}$ mice show impaired localization of leukocytes under nonpathological conditions and impairment of both innate and adaptive immune responses.[8–10]

Consistent with its role in regulating chemotaxis of immune effectors, studies indicate that CCL20 may be involved in various inflammatory disorders. In addition to its potential involvement in psoriasis, inflammatory bowel disease, and asthma, CCL20 has been reported to play a role in various cancers.[11,12] Exploring its potential involvement in renal cell carcinoma (RCC), we observed high levels of CCL20 in patient samples of RCC bone metastasis, which is classically associated with excessive bone resorption. Correspondingly, inflammatory chemokines of the MIP family have been identified as potential mediators of pathological bone loss where MIP-1α and MIP-1δ have been shown to directly enhance osteoclast development.[13,14] Interestingly, genome-wide linkage analyses have identified the genomic locations of both *Ccl20* and *Ccr6* (2q33-37 and

Received in original form October 30, 2015; revised form February 3, 2016; accepted February 13, 2016. Accepted manuscript online Month 00, 2016.
Address correspondence to: Scott L Kominsky, PhD, Department of Orthopaedic Surgery, Johns Hopkins University School of Medicine, 720 Rutland Avenue, Ross 232, Baltimore, MD 21205, USA. E-mail: kominsc@jhmi.edu

*Present address: Department of Orthopaedic Surgery, The Perelman School of Medicine at the University of Pennsylvania, Philadelphia, PA, USA

Additional Supporting Information may be found in the online version of this article.

Journal of Bone and Mineral Research, Vol. xx, No. xx, Month 2016, pp 1–10
DOI: 10.1002/jbmr.2813

6q27, respectively) as regions important for bone quality,[15–17] indicating a potential role for CCL20 in the regulation of bone mass. Although the expression of CCL20 and CCR6 in human bone cells (eg, osteoblast, osteoclast, chondrocyte) has been reported,[18,19] the role of CCL20/CCR6 signaling in bone remains unknown.

Bone disorders (eg, osteoporosis, rheumatoid arthritis, bone metastasis) affect millions of men and women worldwide. Advances in the prevention and treatment of these disorders are dependent on our ability to identify key factors regulating bone formation and remodeling. Here, we investigate the effect of CCL20/CCR6 signaling on bone mass by examining the skeletal phenotype of *Ccr6*$^{-/-}$ and *Ccl20*$^{-/-}$ mice. We demonstrate, for the first time to our knowledge, that loss of CCL20/CCR6 signaling results in reduced trabecular bone volume, coincident with a decrease in osteoblast numbers, potentially stemming from deficiencies in osteoblast maturation, survival, and the recruitment of osteoblast-supporting cells. Taken together, these data indicate that CCL20/CCR6 signaling may represent a novel pathway through which bone accrual and maintenance are regulated.

Materials and Methods

Animals

Animal experiments were carried out in accordance with approved protocols and guidelines of the Johns Hopkins Animal Care and Use Committee. *Ccr6*$^{-/-}$ (B6.129P2-*Ccr6tm1Dgen*/J) mice, backcrossed at least five generations to C57BL/6 mice, were purchased from The Jackson Laboratory (Bar Harbor, ME, USA) and subsequently crossed with C57BL/6 mice (The Jackson Laboratory) to generate the *Ccr6*$^{-/-}$ and WT littermate control mice used in all experiments. To generate *Ccl20*$^{-/-}$ mice, embryonic stem (ES) cells containing a *Ccl20* mutant allele (*Ccl20*^{tm11a}) were obtained from the European Conditional Mouse Mutagenesis Program (Neuherberg, Germany). Within *Ccl20*^{tm11a}, the second exon is flanked by loxP sites and when excised results in a frameshift causing loss of CCL20 mRNA expression (Supplemental Fig. S1). *Ccl20*^{tm11a} ES cells (C57BL/6N) were injected into mouse blastocysts (C57BL/6J) at the Johns Hopkins University School of Medicine Transgenic Core Laboratory to generate chimeric mice. Chimeric mice were bred with C57BL/6J to produce *Ccl20*$^{tm11a/+}$ mice and subsequently crossed with the ubiquitous Cre deleter strain B6.C-Tg(CMV-cre) 1Cgn/J (The Jackson Laboratory), generating heterozygous knockout mice (*Ccl20*$^{+/-}$). *Ccl20*$^{+/-}$ mice were backcrossed to wild-type C57BL/6 mice to remove *Cre* and bred to homozygosity. For genotyping, genomic DNA was extracted from the tails of 3-week-old animals using the Extract-N-Amp Tissue PCR Kit (Sigma-Aldrich, St. Louis, MO, USA) per manufacturer's instructions. Identification of wild-type (WT), heterozygous mutant, and homozygous mutant mice was carried out by allele-specific PCR.

Micro–computed tomography (μCT) and histomorphometry

Femora obtained from 3-, 6-, and 12-week-old *Ccr6*$^{-/-}$, *Ccl20*$^{-/-}$, and WT littermate mice were dissected free of soft tissue and fixed overnight in 70% ethanol. For μCT analysis, femora were scanned using a SkyScan 1172 high-resolution μCT scanner (Bruker microCT, Kontich, Belgium). Image reconstruction (NRecon v1.6), data analysis (CTAn v1.9), and three-dimensional model visualization (CTVol v2.0) software (Bruker microCT) were utilized to analyze bone structure in accordance with the recommendations of the American Society of Bone and Mineral Research.[20,21] For histomorphometric analysis, 8-week-old *Ccr6*$^{-/-}$ and WT littermate mice received injections of 1% (wt/vol) calcein at 8 and 3 days before euthanization. Femurs were embedded in polymethyl methacrylate for sectioning and analyzed using a semiautomatic method (Osteoplan II, Kontron, Poway, CA, USA).

Cell isolation and culture

Bone marrow was isolated from female *Ccr6*$^{-/-}$, *Ccl20*$^{-/-}$, and WT littermate mice as previously described.[14] T cells were isolated from total bone marrow using the CD4^{+} CD25^{+} T Cell Isolation Kit (Miltenyi Biotec, Bergisch Gladbach, Germany) per manufacturer's instructions. To generate bone marrow macrophages (BMM), marrow cells were washed and resuspended in complete media (αMEM + 10% fetal bovine serum [FBS] + 1% penicillin/streptomycin) containing 5 ng/mL macrophage colony-stimulating factor (M-CSF; R&D Systems, Minneapolis, MN, USA) and incubated in a 100-mm dish overnight. Nonadherent cells were then collected, strained through 70-μm nylon mesh, and treated with 50 ng/mL M-CSF for 3 days to generate M-CSF-dependent BMM. To generate BMSC, marrow cells were washed and resuspended in complete media and incubated overnight. Adherent cells were collected as BMSC, and cell purity was confirmed >95% negative for nonspecific esterase (a marker for cells of the monocyte/macrophage lineage).

To determine the number of BMSC contained within the bone marrow, marrow was plated at clonal density, incubated in complete medium for 10 to 14 days, and colony formation was assessed by methylene blue dye staining. To determine the osteogenic potential of BMSC within the bone marrow, marrow was plated at clonal density, incubated in osteogenic medium (complete media containing dexamethasone [10^{-8} M], ascorbic acid [50 μg/mL], and β-glycerolphosphate [5mM]) for up to 18 days, and alkaline phosphatase positive colony formation was assessed by alkaline phosphatase staining. For osteoclast differentiation, BMM were cultured in complete media containing M-CSF (20 ng/mL) and receptor activator of NF-κB ligand (RANKL; 5 ng/mL; R&D Systems) for a period of 7 days. Fifty percent of the culture media was replaced with fresh complete media containing cytokines every 3 days. For osteoblast differentiation, BMSC were cultured in osteogenic media for up to 21 days with biweekly media changes. Calcium deposition was visualized by alizarin red staining and quantified by measuring stain intensity via microtiter plate reader at 490 nm (Bio-Rad, Hercules, CA, USA).

Quantitative (q)PCR

Total RNA was extracted using Trizol (ThermoFisher Scientific, Grand Island, NY, USA) and cDNA was generated by reverse transcription. Twenty-five-microliter reactions contained 1X SYBR Green Reaction Mix (ThermoFisher Scientific), 1 μL cDNA, and 100 nm of each primer: CCR6 (sense) 5′-TTGTCCTCACCCTACCGTTC-3′, (antisense) 5′-AGGGCTTGAGATGATGATGG-3′; CCL20 (sense) 5′-CGACTGTTGCCTCTCGTACA-3′, (antisense) 5′-AGGAGGTTCACAGCCCTTTT-3′; Runx2 (sense) 5′-TTCAACGATCTGAGATTTGTGGG-3′ (antisense) 5′-GGATGAGGAATGCGCCCTA-3′; osterix (sense) 5′-ATGGCGTCCTCTCTGCTTG-3′ (antisense) 5′-TGAAAGGTCAGCGTATGGCTT-3′; alkaline phosphatase (sense) 5′-GGCTGGAGATGGACAAATTCC-3′ (antisense) 5′-GGACCTGAGCGTTGGTGTTA-3′; bone sialoprotein (sense) 5′-AGGGAGGCAGTGACTCTTCAG-3′ (antisense)

5′-CTTCGGAACTATCGCCGTCTC-3′; type I collagen (sense) 5′-TG TTCAGCTTTGTGGACCTC-3′ (antisense) 5′-TCTTTGGGGGTTGGG ACAGT-3′; osteocalcin (sense) 5′-ATGAGGACCATCTTTCTGCT-3′ (antisense) 5′-ATAGTGATACCGTAGATGCG-3′; GAPDH (sense) 5′-AACTTTGGCATTGTGGAAGG-3′, (antisense) 5′-ACACATTGG GGGTAGGAACA-3′. qRT-PCR parameters were: 1 cycle (95°C for 3 minutes) and 40 cycles (95°C for 30 seconds, 61.9°C for 30 seconds, and 72°C for 45 seconds). Amplification of GAPDH was used as an internal control. Relative expression between samples was calculated by the comparative C_T method.

Western analysis

Total protein was extracted from cells using lysis buffer consisting of 15% glycerol, 5% SDS, and 250 mM Tris-HCl, pH 6.7. Equal amounts of protein were resolved using 10% SDS-PAGE. Protein was transferred to ECL nitrocellulose membranes (GE Healthcare Bio-Sciences, Pittsburgh, PA, USA) and probed with anti-CCR6 (Enzo Life Sciences, Farmingdale, NY, USA), anti-phospho-PI3K (Cell Signaling, Danvers, MA, USA), anti-PI3K (Cell Signaling), anti-phospho-AKT (Cell Signaling), anti-AKT (Cell Signaling), anti-caspase 3 (Cell Signaling), and β-actin (Sigma-Aldrich) antibodies. Membranes were then incubated with horseradish peroxidase-conjugated antibody against rabbit IgG (GE Healthcare Bio-Sciences), and binding was revealed by chemiluminescence (GE Healthcare Bio-Sciences).

Immunohistochemical analysis

Paraffin-embedded sections were deparaffinized in xylene and rehydrated through graded ethanol. Antigen retrieval was achieved by immersing sections in 0.01 mol/L sodium citrate (pH 6.0) and heating in a steamer for 20 minutes. Sections were cooled to room temperature (RT), and endogenous peroxidase activity was quenched by immersing in 0.3% hydrogen peroxide. For CCL20: blocking was carried out by incubation in Serum-free Protein Block (Dako, Carpinteria, CA, USA) as per the manufacturer's instructions. Sections were then incubated with rabbit polyclonal anti-CCL20 (Abcam, Cambridge, MA, USA) for 16 hours at 4°C. Diluted biotinylated anti-rabbit IgG (Vector Laboratories, Burlingame, CA, USA) was added to the sections and incubated for 30 minutes at RT followed by Vectastain ABC reagent (Vector Laboratories). CCL20 protein was visualized using 3, 3′-diaminobenzidine (DAB) as per the manufacturer's instructions (Vector Laboratories). Sections were subsequently washed in water and counterstained in hematoxylin (ThermoFisher Scientific). For CCR6: blocking was carried out by incubation in Serum-free Protein Block (Dako) per the manufacturer's instructions. Sections were then incubated with hamster polyclonal anti-CCR6 (Biolegend, San Diego, CA, USA) conjugated to Alexafluor 647 and rabbit polyclonal anti-osteocalcin (Santa Cruz Biotechnology, Dallas, TX, USA) for 16 hours at 4°C. Cells were then incubated with anti-rabbit IgG conjugated to Alexafluor 488 (ThermoFisher Scientific) for 1 hour at room temperature. Sections were stained with Hoechst (ThermoFisher Scientific) to allow visualization of cell nuclei. Images of CCL20 and CCR6 were acquired by light and fluorescence microscopy, respectively.

ELISA

Cells were plated at 2×10^5 cells/well in 6-well plates in appropriate medium for 48 hours. Conditioned media was collected and levels of CCL20 were analyzed by ELISA using a mouse CCL20 immunoassay kit (R&D Systems) per manufacturer's instruction. For measurement of osteocalcin and CTX-I, serum was collected from 8-week-old mice and the levels of osteocalcin and CTX-I were analyzed by ELISA using the Mouse Osteocalcin (Biomedical Technologies, Stoughton, MA, USA) and RatLaps (Immunodiagnostic Systems, Fountain Hills, AZ, USA) EIA kits, respectively, per manufacturer's instruction. For measurement of cyclic (c)AMP, BMSC were isolated from WT C57BL/6 mice and cultured in osteogenic media for 7 days. Cells were washed in PBS and cultured in media containing 0.1% FBS overnight. Amounts of 1 μM forskolin (Sigma-Aldrich), 100 ng/mL CCL20 (R&D Systems), and 100 ng/mL pertussis toxin (Sigma-Aldrich) were then added alone or in combination for 30 minutes, and cAMP levels were analyzed by ELISA using the cAMP EIA kit (Cayman Chemical, Ann Arbor, MI, USA), per manufacturer's instruction.

Migration assay

BMM or T cells were suspended in complete medium and added to the upper chamber of transwell filter units with 5-μm pore size (Corning, NY, USA). Inserts were then placed into the lower chambers of transwell units containing osteoblasts (BMSC previously cultured in osteogenic media), conditioned media obtained from osteoblasts, CCL20 (1 pg/mL), or complete medium alone. Transwell units were then incubated at 37°C for 24 hours, fixed in methanol, and cells on the upper side of the transwell filter were removed with a cotton swab. Filters were stained with 0.5% toluidine blue and migrated cells were counted by light microscopy.

Survival assay

BMSC were cultured in osteogenic media to induce osteoblast differentiation. Osteogenic media was subsequently replaced with complete media ± CCL20 (100 ng/mL) and cells were incubated for 24 hours. Cell culture was continued in complete media or under starvation conditions (0.1% FBS) in the presence or absence of CCL20 for 24 hours. Cells were then harvested and total protein was extracted for Western analysis.

Proliferation assay

Cell proliferation was determined by MTS assay. Cells were incubated in a 96-well plate for the desired time periods and MTS (0.2 mg/mL) (Promega, Madison, WI, USA) and phenazine ethosulfate (30 μM) (Sigma-Aldrich) were subsequently added to each well. Plates were then incubated at 37°C for 2 hours and the conversion of MTS to formazan by metabolically viable cells was monitored using a 96-well microtiter plate reader at 490 nm (Bio-Rad).

Statistical analysis

Comparison between groups was conducted by unpaired, two-tailed Student's *t* test using Prism 4 software (GraphPad Software, La Jolla, CA, USA). All results are reported as the mean ± the standard error of the mean (SEM). Any p values <0.05 were considered significant. For all figures, (*) denotes $p < 0.05$, (**) denotes $p < 0.01$, and (***) denotes $p < 0.001$.

Results

Global deletion of *Ccr6* reduces bone mass

To begin assessing the impact of CCL20/CCR6 signaling on bone, we utilized mice harboring a global deletion of *Ccr6*. Because

CCR6 and CCL20 are reported to interact monogamously, this model is predicted to prevent all manner of CCL20 and CCR6 signaling. We initially examined the skeletal phenotype of female *Ccr6*$^{-/-}$ mice relative to age- and sex-matched WT littermate control mice by quantitative μCT analysis. Although no differences in animal size or femur length were observed (data not shown), femora of *Ccr6*$^{-/-}$ mice demonstrated a greater than 37% reduction in trabecular bone volume at age 3 weeks that was maintained at 6 and 12 weeks relative to WT controls (Fig. 1*A*, *B*). Further, the decrease in trabecular bone volume was coincident with significant decreases in trabecular number and thickness, along with a significant increase in trabecular separation (Fig. 1*C–E*). A 10% reduction in cortical bone volume was also observed in femora of 3-week-old *Ccr6*$^{-/-}$ mice. However, in contrast to the effects observed in trabecular bone, this difference was not maintained at 6 and 12 weeks, and no differences in cortical thickness were observed (Fig. 1*F–H*). Similar effects on bone mass were observed in male mice (Supplemental Fig. S2), although the reduction in cortical bone volume remained evident at 12 weeks.

To characterize the molecular and cellular changes associated with the reduction in trabecular bone volume, histomorphometric analysis was performed on femora of 8-week-old female *Ccr6*$^{-/-}$ and WT mice. Consistent with the reduction in bone volume observed by μCT analysis, osteoblast numbers were significantly decreased in *Ccr6*$^{-/-}$ relative to WT mice as indicated by a 69% reduction in osteoblast number/bone length (Fig. 1*I*). Correspondingly, osteoid deposition was also significantly lower with a 71% reduction in osteoid volume/tissue volume, 61% reduction in osteoid surface/bone surface, and 43% reduction in osteoid thickness (Fig. 1*J–L*). In line with reduced bone volume and osteoblast numbers, *Ccr6*$^{-/-}$ mice demonstrated significantly lower serum levels of the bone-formation marker osteocalcin relative to WT controls as measured by ELISA (Fig. 1*M*). Notably, the mineral apposition rate was unchanged in *Ccr6*$^{-/-}$ relative to WT mice (Fig. 1*N*), indicating that although the number of osteoblasts is reduced in *Ccr6*$^{-/-}$ mice, those present function at a level similar to that in WT mice. In contrast to the pronounced effect on osteoblast numbers, no significant difference was observed in the number of osteoclasts in *Ccr6*$^{-/-}$ versus WT mice (Fig. 1*O*). Moreover, *Ccr6*$^{-/-}$ mice demonstrated reduced serum levels of C-telopeptide of type I collagen (CTX-I) relative to WT controls, indicating reduced osteoclast activity (Fig. 1*P*), incongruent with the observed reduction in bone mass. Taken together, these data demonstrate that the loss of *Ccr6* results in a marked bone

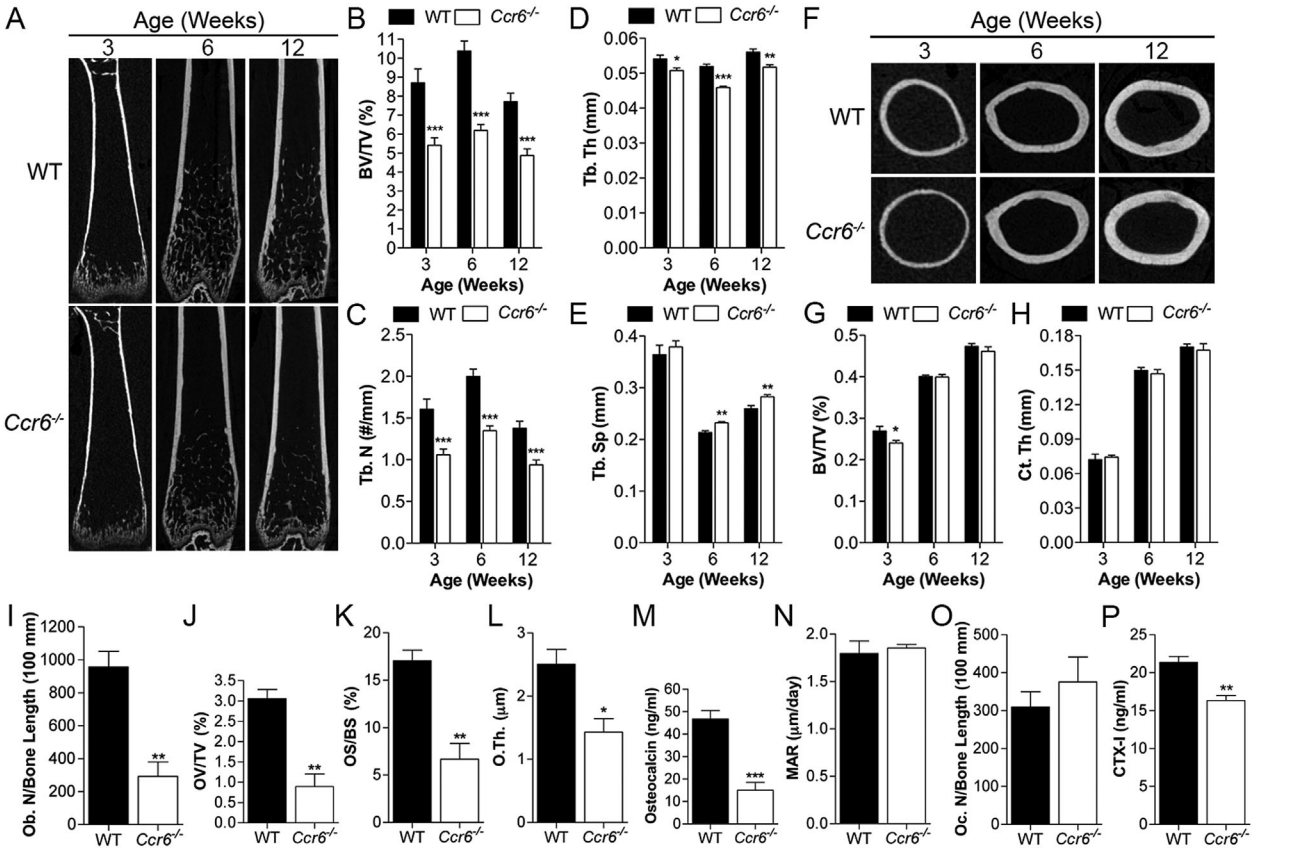

Fig. 1. Effect of *Ccr6* loss on bone mass. (*A–H*) Femora obtained from 3-, 6-, and 12-week-old female *Ccr6*$^{-/-}$ and wild-type (WT) mice were analyzed by quantitative μCT analysis. (*A*) Representative images of trabecular bone. (*B*) Trabecular bone volume/tissue volume (BV/TV). (*C*) Trabecular number (Tb.N). (*D*) Trabecular thickness (Tb.Th). (*E*) Trabecular separation (Tb.Sp). (*F*) Representative images of cortical bone. (*G*) Cortical BV/TV. (*H*) Cortical thickness (Ct.Th). (*I–L, N, O*) Histomorphometric analysis of the distal femur was conducted in 8-week-old female *Ccr6*$^{-/-}$ and WT mice. (*I*) Osteoblast number (Ob.N)/bone length. (*J*) Osteoid volume/tissue volume (OV/TV). (*K*) Osteoid surface/bone surface (OS/BS). (*L*) Osteoid thickness (O.Th). (*N*) Mineral apposition rate (MAR). (*O*) Osteoclast number (Oc.N)/bone length. (*M, P*) Protein levels of osteocalcin and CTX-I in the serum of 8-week-old *Ccr6*$^{-/-}$ and WT mice were determined by ELISA. Data are reported as the mean ± SEM. For *A–P*, $n \geq 8$/age group. $^{*}p < 0.05$; $^{**}p < 0.01$; $^{***}p < 0.001$.

phenotype characterized by reduced trabecular bone volume and decreased osteoblast numbers.

Expression of CCL20 and CCR6 increases during osteoblast differentiation

To elucidate the contribution of CCL20/CCR6 signaling toward the low-bone phenotype observed in *Ccr6*$^{-/-}$ mice, we first examined the expression of CCL20 and CCR6 in cells regulating bone formation and homeostasis. Expression of CCR6 was detected at similar levels in bone marrow macrophages (BMM), a common source of osteoclast precursors, before and after differentiation in the presence of M-CSF and RANKL, whereas CCL20 expression was not detectable in either condition (Fig. 2*A*). Albeit at low levels, CCL20 and CCR6 were both expressed in bone marrow stromal cells (BMSC), a common source of osteoblast, chondrocyte, and adipocyte precursors. Notably, levels of CCL20 and CCR6 increased significantly after differentiation of BMSC toward the osteoblast lineage (Fig. 2*B*), beginning early in the differentiation process and escalating toward maturity (Fig. 2*C–E*). In contrast, little to no change in CCL20 or CCR6 expression occurred after differentiation toward the chondrocyte or adipocyte lineages (Fig. 2*B*). Correspondingly, CCL20 and CCR6 protein was readily detected in osteoblasts residing in the murine femur by immunohistochemical (IHC) analysis, whereas levels in bone marrow, osteocytes, and chondrocytes were low/absent (Fig. 2*F*, *G*). In aggregate, these data indicate that CCL20 and CCR6 are present in both developing and mature osteoblast populations, increasing during differentiation.

CCR6 is coupled to $G\alpha_i$ and $G\alpha_q$ in osteoblasts

CCR6 is a seven-transmembrane domain receptor reportedly coupled to $G\alpha_i$ in intestinal epithelial cells and $G\alpha_q$ in natural killer cells;[22] however, its signaling in osteoblasts has not been explored. Thus, we next examined whether CCR6 acts as a functional G protein–coupled receptor (GPCR) in osteoblasts. Because $G\alpha_s$ and $G\alpha_i$ signaling are known to activate and inhibit the cyclic adenosine monophosphate (cAMP)-generating enzyme adenylate cyclase, respectively, we began by examining the ability of CCL20 to modulate cAMP levels. BMSC obtained from WT mice were cultured in osteogenic media to generate mature osteoblasts. Upon treatment with forskolin, a potent stimulator of cAMP production, cAMP levels were significantly induced (Fig. 3*A*). Consistent with signaling through $G\alpha_i$, CCL20 inhibited the induction of cAMP by forskolin. Moreover, the inhibitory effect of CCL20 on cAMP levels was reversed by pertussis toxin, a known antagonist of $G\alpha_i$ signaling. Because many GPCRs are capable of activating more than one $G\alpha$ subtype, we next examined the ability of CCL20 to activate $G\alpha_q$. To accomplish this task, we focused on the PI3K-AKT pathway, a

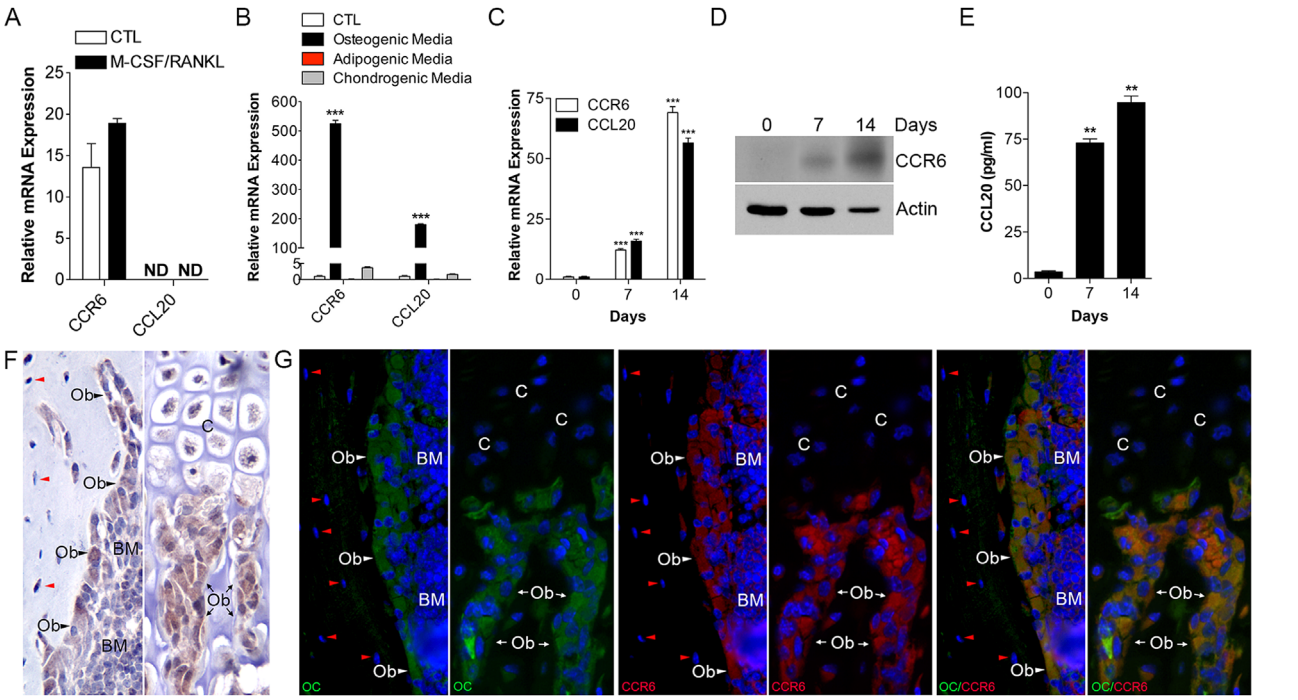

Fig. 2. Expression of CCL20 and CCR6 in bone cells. (*A*) BMM were cultured in the presence or absence of M-CSF/RANKL. (*B–E*) BMSC were cultured in the presence or absence of (*B–E*) osteogenic, (*B*) adipogenic, or (*B*) chondrogenic media. (*A–C*) CCL20 and CCR6 mRNA expression was determined by qRT-PCR. ND = not detected. (*D*) Protein levels of CCR6 in total cell lysates were determined by Western analysis. Representative blot from 2 independent experiments. (*E*) Protein levels of CCL20 in conditioned media were determined by ELISA. Data for *A–C* and *E* are representative of ≥3 independent experiments, $n = 3$. Data are reported as the mean ± SEM. $^{**}p < 0.01$; $^{***}p < 0.001$. (*F*) CCL20 expression in murine femora was determined by immunohistochemical staining, $n = 3$. Proteins were identified using DAB (brown) and visualized by light microscopy (×200). (*G*) CCR6 and osteocalcin (OC) expression in murine femora was determined by immunofluorescent labeling with red and green fluorophores, respectively, and presented as individual and composite images (yellow = co-localization of CCR6 and osteocalcin in osteoblasts) obtained by fluorescence microscopy (×200), $n = 3$. Ob = osteoblast; C = chondrocyte; BM = bone marrow; red arrowheads = osteocytes.

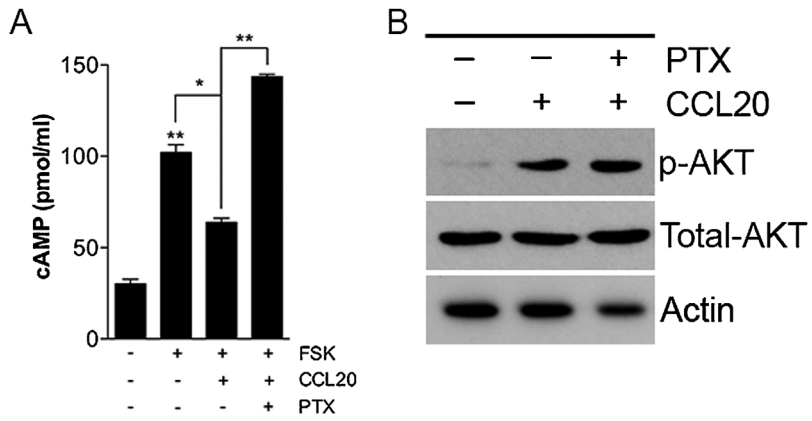

Fig. 3. Ability of *Ccl20* to activate G protein signaling in osteoblasts. (*A*) Murine osteoblasts were cultured in the presence or absence of 1 μM forskolin (FSK), 100 ng/mL CCL20, and 100 ng/mL pertussis toxin (PTX). Protein levels of cAMP were determined by ELISA. Data are representative of 3 independent experiments, $n = 3$, and are reported as the mean ± SEM. $^{*}p < 0.05$; $^{**}p < 0.01$. (*B*) Murine osteoblasts were cultured in the presence or absence of CCL20 (100 ng/mL) and PTX (100 ng/mL). Levels of phosphorylated (p) and total AKT were determined by Western analysis. Representative blot from 3 independent experiments.

downstream target of $G\alpha_q$, as well as the $G\beta\gamma$ subunit released upon $G\alpha_i$ activation. Stimulation of osteoblasts with CCL20 resulted in phosphorylation of AKT, indicating induction of the PI3K-AKT pathway (Fig. 3*B*). Because $G\alpha_q$ signaling is insensitive to pertussis toxin, unlike $G\alpha_i$, we determined whether pertussis toxin could inhibit CCL20-induced AKT phosphorylation. In contrast to its effects on CCL20-mediated repression of cAMP levels, pertussis toxin did not inhibit the phosphorylation of AKT by CCL20, indicating activation of $G\alpha_q$. Overall, these data indicate that CCR6 is a functional GPCR in osteoblasts, coupled to both $G\alpha_i$ and $G\alpha_q$.

Ccr6 loss delays osteoblast maturation

Because CCL20 and CCR6 are co-expressed in the osteoblast lineage, both autocrine and paracrine signaling events could contribute to the decreased osteoblast numbers and trabecular bone volume observed in *Ccr6*$^{-/-}$ mice. Investigating potential autocrine actions, we first examined the effect of *Ccr6* loss on the proliferation and differentiation of osteoblast precursors. To determine whether *Ccr6* loss affected the growth rate of osteoblast precursors, BMSC from *Ccr6*$^{-/-}$ and WT mice were cultured in complete media and proliferation was assessed over 96 hours. As measured by MTS assay, no difference in the growth rate of *Ccr6*$^{-/-}$ BMSC was observed relative to WT BMSC (Fig. 4*A*). Next, we examined the effect of *Ccr6* loss on the number of BMSC contained within the bone marrow. Equivalent cell densities of *Ccr6*$^{-/-}$ and WT bone marrow were cultured in complete media and colony formation was assessed after methylene blue staining. As observed in Fig. 4*B*, an equal number of colonies formed in cultures of *Ccr6*$^{-/-}$ and WT bone marrow, suggesting that *Ccr6* loss does not affect the number of BMSC present.

Lastly, we examined whether *Ccr6* loss impacts the osteogenic potential of BMSC. After culture of *Ccr6*$^{-/-}$ and WT bone marrow in osteogenic media to promote differentiation toward the osteoblast lineage, a significant reduction in alkaline phosphatase-positive colony formation was observed in *Ccr6*$^{-/-}$ versus WT cultures (Fig. 4*B*), indicating a potential delay in osteoblast maturation. To examine the rate of osteoblast maturation, equal numbers of *Ccr6*$^{-/-}$ and WT BMSC were cultured in osteogenic media and matrix mineralization was assessed at various time points along with the expression of genes regulating and demarcating osteoblast differentiation. Although matrix mineralization occurred in both *Ccr6*$^{-/-}$ and WT BMSC cultures, a significant delay was observed in *Ccr6*$^{-/-}$ cultures at 10 days post differentiation by alizarin red staining (Fig. 4*C*). Correspondingly, expression of Runx2 and osterix, two central regulators of osteoblast differentiation, was significantly delayed in *Ccr6*$^{-/-}$ versus WT cultures beginning 4 days post differentiation and continuing through day 10 (Fig. 4*D*). Further, the delay in Runx2 and osterix expression in *Ccr6*$^{-/-}$ cultures was accompanied by similar delays in the expression of the osteoblast marker genes alkaline phosphatase, bone sialoprotein, type I collagen, and osteocalcin (Fig. 4*D*). Collectively, these data indicate that osteoblast maturation is delayed by the absence of *Ccr6*, consistent with the reduced osteoblast numbers and trabecular bone volume observed in *Ccr6*$^{-/-}$ mice.

CCL20/CCR6 signaling promotes osteoblast survival

In addition to their ability to stimulate chemotaxis, homeostatic chemokines such as CCL20 have been reported to increase survival in various cell types.[23,24] Continuing our investigation of autocrine CCL20/CCR6 signaling events with the potential to impact osteoblast numbers, we assessed the ability of CCL20 to promote osteoblast survival. After culture under starvation conditions, osteoblasts derived from both *Ccr6*$^{-/-}$ and WT mice underwent apoptosis as evidenced by increased levels of cleaved caspase-3 (Fig. 5*A*). Notably, CCL20 treatment of WT osteoblasts prevented apoptosis as cleavage of caspase-3 was markedly reduced relative to untreated cells. In contrast, treatment with CCL20 did not provide any protective effect in osteoblasts from *Ccr6*$^{-/-}$ mice where cleaved caspase-3 levels were similar to that observed in untreated cells. Consistent with the observed anti-apoptotic effect, treatment of WT osteoblasts with CCL20 resulted in PI3K-AKT activation as evidenced by increased phosphorylation of PI3K and AKT, whereas no activation was observed in osteoblasts derived from *Ccr6*$^{-/-}$ mice (Fig. 5*B*). Given the known role of PI3K-AKT signaling in regulating survival, these findings suggest that CCL20 may

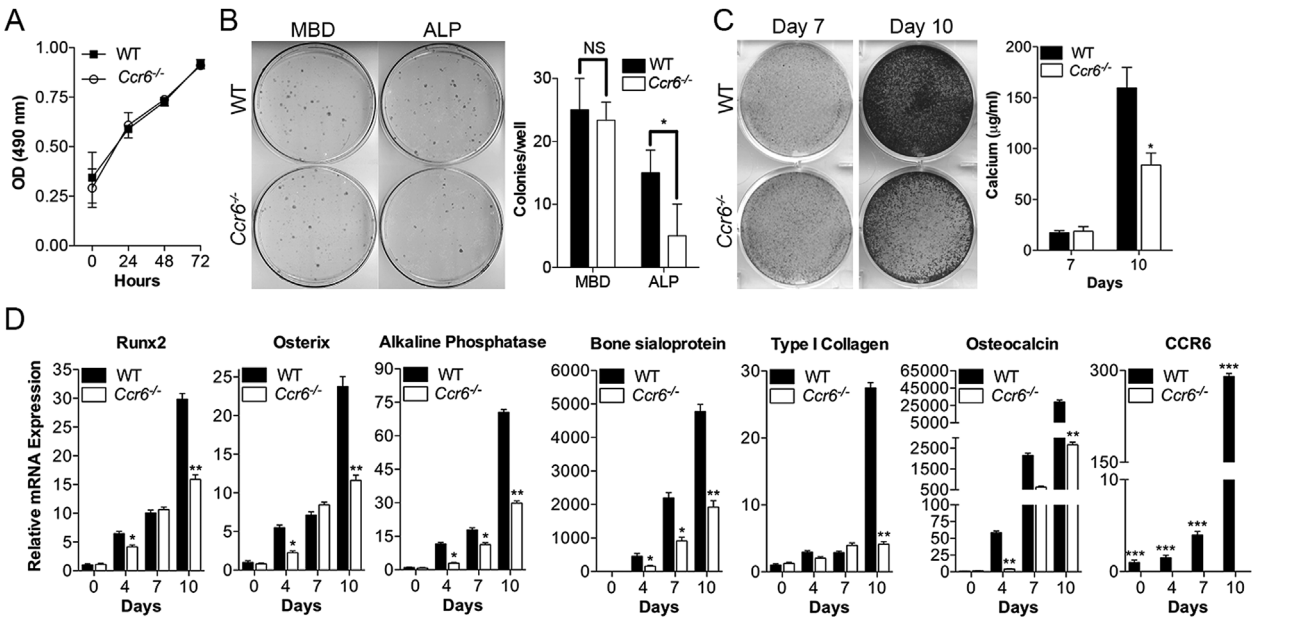

Fig. 4. Effect of *Ccr6* loss on osteoblast development. (*A*) BMSC were isolated from bone marrow, cultured in complete media, and proliferation was assessed by MTS assay. (*B*) Bone marrow was plated at clonal density in complete or osteogenic media. Colony formation was examined by visualization (left) and quantification (right) of methylene blue dye (MBD) and alkaline phosphatase (ALP) staining for the determination of BMSC quantity and osteogenic potential, respectively. NS = not significant. (*C, D*) BMSC were cultured in osteogenic media and differentiation was examined by (left) visualization and (right) quantification of alizarin red staining and (*D*) by assessment of osteoblast marker gene expression via qPCR. Data for *A–D* are representative of ≥3 independent experiments, $n = 3$. Data are reported as the mean ± SEM. $^{*}p < 0.05$; $^{**}p < 0.01$; $^{***}p < 0.001$.

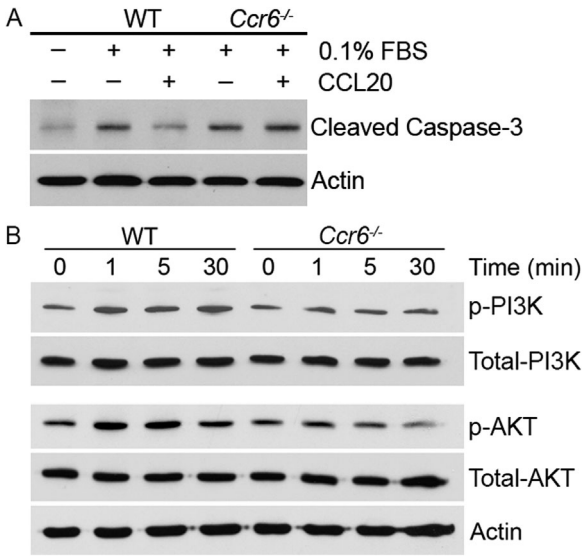

Fig. 5. Effect of CCL20 on osteoblast survival. (*A*) Murine osteoblasts were cultured in the presence or absence of CCL20 (100 ng/mL) under starvation or non-starvation conditions. Protein levels of cleaved caspase-3 in total cell lysates were determined by Western analysis. (*B*) Murine osteoblasts were cultured under starvation conditions and subsequently stimulated with CCL20 (100 ng/mL). Cells were harvested at various time points and levels of phosphorylated (p) and total PI3K and AKT were determined by Western analysis. Data for *A, B* are representative of 3 independent experiments.

exert a protective effect on osteoblasts, mediated though the activation of AKT.

CCL20/CCR6 signaling promotes recruitment of osteoblast-supporting cells

Because osteoblasts appear to be a significant source of CCL20 in the bone environment (Fig. 2*F*) and CCL20 is known to exert chemotactic effects in a variety of cell types, we also examined the possibility that the reduced osteoblast numbers in *Ccr6*$^{-/-}$ mice were in part owing to the ability of osteoblast-derived CCL20 to recruit supporting cells through paracrine actions. CCR6 is expressed on several cell types commonly found in the bone marrow environment, including macrophages and T cells. Given the reported ability of BMM and T cells to facilitate osteoblast differentiation and survival,[25–31] we examined the ability of CCL20 to promote the recruitment of these cells. BMM or T cells isolated from *Ccr6*$^{-/-}$ and WT mice were plated in the top chamber of transwell filter units, whereas CCL20, osteoblasts, or osteoblast-conditioned media were placed in the lower chamber. CCL20 induced migration of both WT BMM and T cells, whereas *Ccr6*$^{-/-}$ cells were unaffected (Fig. 6*A, B*). Supporting a role for osteoblast-derived CCL20 in this process, although the presence of osteoblasts or osteoblast-conditioned media in the lower chamber stimulated migration of BMM and T cells from both WT and *Ccr6*$^{-/-}$ mice, recruitment of *Ccr6*$^{-/-}$ cells was significantly inhibited relative to WT cells. Taken together, these data indicate that CCL20, among other factors produced by osteoblasts, has the ability to stimulate the recruitment of BMM and T cells, representing another

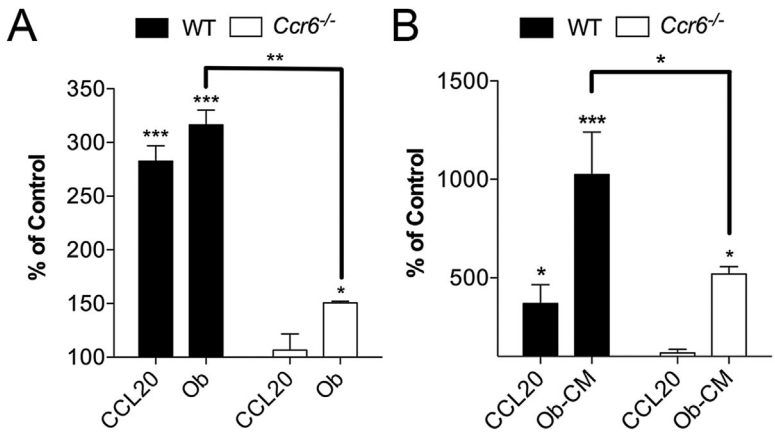

Fig. 6. Effect of osteoblast-derived CCL20 on BMM and T-cell recruitment. (*A*) Murine BMM were loaded into the top chamber of transwell filter units and migration toward media alone, CCL20 (1 pg/mL), or osteoblasts (Ob) in the lower chamber was determined. (*B*) Murine T cells were loaded into the top chamber of transwell filter units and migration toward media alone, CCL20 (1 pg/mL), or osteoblast-conditioned media (Ob-CM) in the lower chamber was determined. Data for *A, B* are representative of 2 independent experiments, $n = 3$. Data are reported as the mean % of control (migration in the presence of media alone) $\pm$ SEM. $^{*}p < 0.05$; $^{**}p < 0.01$; $^{***}p < 0.001$.

potential event contributing to the reduced osteoblast numbers and trabecular bone volume observed in *Ccr6*$^{-/-}$ mice.

Global deletion of *Ccl20* reduces trabecular bone mass

To this point, the principal findings of our study have stemmed from observations made using *Ccr6*$^{-/-}$ mice. Operating under the premise that CCL20 and CCR6 interact in a monogamous fashion, it is presumed that these results were attributable to the loss of CCL20 signaling. Although this is generally supported by the literature, it remained possible that our results were reflective of signaling initiated by non-chemokine or as yet undiscovered ligands of CCR6.[32] To address this possibility, we generated mice harboring a global deletion of *Ccl20* and examined their skeletal phenotype relative to age- and sex-matched WT littermate control mice by quantitative μCT analysis. Similar to our observations in *Ccr6*$^{-/-}$ mice, femora of female *Ccl20*$^{-/-}$ mice demonstrated a greater than 45% reduction in trabecular bone volume at 3 weeks of age that was maintained at 6 and 12 weeks relative to WT controls (Fig. 7*A, B*). Further, the decrease in trabecular bone volume was

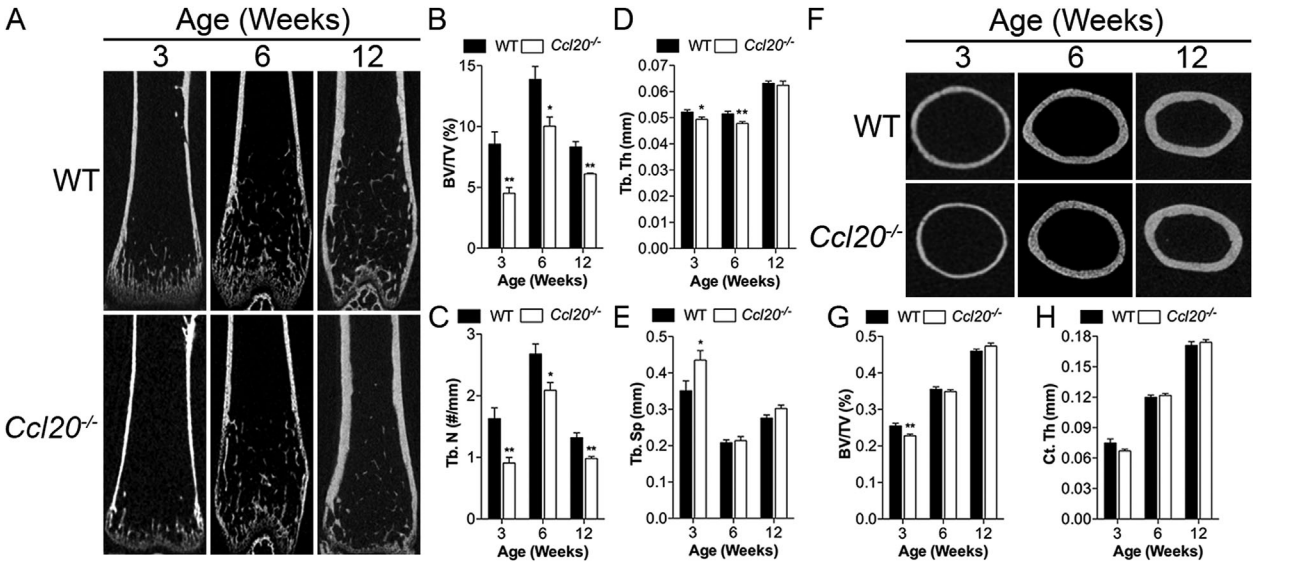

Fig. 7. Effect of *Ccl20* loss on bone mass. (*A–H*) Femora obtained from 3-, 6-, and 12-week-old female *Ccl20*$^{-/-}$ and wild-type (WT) mice were analyzed by quantitative μCT analysis. (*A*) Representative images of trabecular bone. (*B*) Trabecular bone volume/tissue volume (BV/TV). (*C*) Trabecular number (Tb.N). (*D*) Trabecular thickness (Tb.Th). (*E*) Trabecular separation (Tb.Sp). (*F*) Representative images of cortical bone. (*G*) Cortical bone volume/tissue volume (BV/TV). (*H*) Cortical thickness (Ct.Th). Data are reported as the mean $\pm$ SEM. $n \geq 8$/age group. $^{*}p < 0.05$; $^{**}p < 0.01$.

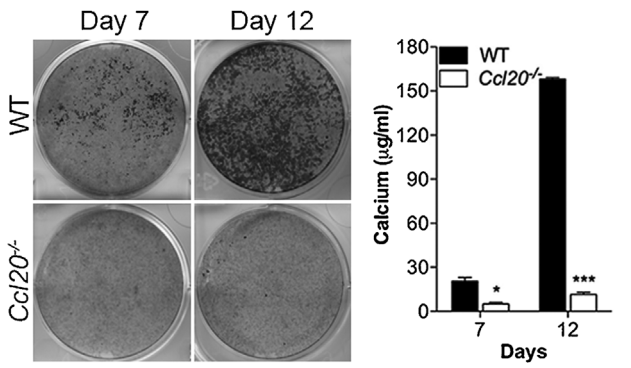

Fig. 8. Effect of *Ccl20* loss on osteoblast development. BMSC were cultured in osteogenic media and differentiation was examined by (left) visualization and (right) quantification of alizarin red staining. Data are representative of 2 independent experiments, $n = 3$. Data are reported as the mean ± SEM. $^{*}p < 0.05$; $^{***}p < 0.001$.

coincident with significant decreases in trabecular number and thickness, along with a significant increase in trabecular separation (Fig. 7*C–E*). Although cortical bone volume was reduced at 3 weeks of age, this difference was not maintained because no differences in either cortical bone volume or thickness were observed at 6 or 12 weeks (Fig. 7*F–H*), consistent with observations in *Ccr6*$^{-/-}$ mice. Also similar to *Ccr6*$^{-/-}$ mice, *Ccl20*$^{-/-}$ mice did not demonstrate any differences in animal size or femur length, and comparable results were obtained in male animals (Supplemental Fig. S3). Moreover, BMSC isolated from *Ccl20*$^{-/-}$ mice demonstrated delayed osteoblast maturation in vitro (Fig. 8). Collectively, these data demonstrate that *Ccl20*$^{-/-}$ mice exhibit reduced trabecular bone volume akin to that observed in *Ccr6*$^{-/-}$ mice, indicating that this phenomenon is regulated by CCL20 signaling through CCR6.

Discussion

The goal of the present study was to gain insight into the role of the CCL20/CCR6 axis in the accrual of bone mass. We demonstrated for the first time to our knowledge that deletion of *Ccr6* in mice results in a significant reduction in trabecular bone volume, likely secondary to a decrease in osteoblast numbers. The lower osteoblast numbers together with unchanged mineral apposition rate observed in *Ccr6*$^{-/-}$ versus WT mice suggests impairment in osteoblast maturation rather than osteoblast function. This was further supported by in vitro studies revealing delays in the differentiation of *Ccr6*$^{-/-}$ versus WT osteoblast progenitors, with no apparent effect on their quantity in bone marrow or proliferation rate. Further, the reduced trabecular bone volume in *Ccr6*$^{-/-}$ mice does not appear to be related to changes in bone resorption as neither osteoclast number or activity was elevated. Recently, the anti-microbial peptide β-defensin 2 has been reported to be a non-chemokine ligand for CCR6, calling into question the involvement of CCL20 in various CCR6 functions.[32] Importantly, we also found that the reduced trabecular bone volume observed in *Ccr6*$^{-/-}$ mice was recapitulated in *Ccl20*$^{-/-}$ mice, confirming that this bone phenotype was the product of disrupting CCL20/CCR6 signaling. To our knowledge, this represents the first in vivo evidence that loss of CCL20 can "phenocopy" the loss of CCR6, although further studies are needed to confirm this relationship with respect to other functions attributed to the CCL20/CCR6 axis (eg, immune response).

Although the ultimate mechanism responsible for the low-bone phenotype observed in *Ccr6*$^{-/-}$ and *Ccl20*$^{-/-}$ mice is yet to be determined, our studies indicate that osteoblasts are a significant source of CCL20 in the bone environment and that CCR6 is present in both developing and mature osteoblast populations, highlighting the potential of osteoblast-initiated CCL20/CCR6 signaling to contribute through both autocrine and paracrine actions. Supporting potential autocrine effects, we provide evidence that CCR6 acts as a functional G protein–coupled receptor in osteoblasts and promotes osteoblast differentiation and survival. With respect to potential paracrine effects, CCR6 expression has been reported in various immune cells found within the bone environment, and CCL20 has been shown to stimulate chemotaxis in these cells.[5–7] Our data indicate that osteoblasts are able to recruit both BMM and T cells, at least in part through CCL20/CCR6 signaling. Given the reported ability of BMM and T cells to promote osteoblast differentiation and survival,[26,29,33] diminished recruitment of these immune cells may also contribute to the observed low-bone phenotype. Given the multitude of possible signaling events and cell types involved, conditional deletion of *Ccl20* and *Ccr6* in specific cell lineages will be important to fully establish the mechanisms responsible for the reduced trabecular bone mass and osteoblast numbers occurring in *Ccr6*$^{-/-}$ and *Ccl20*$^{-/-}$ mice.

Given that several studies have reported a potential role for MIP family members (eg, CCL3, CCL15), including CCL20, in mediating pathological bone loss by promoting osteoclast formation,[13,14] our discovery that loss of CCL20/CCR6 signaling results in reduced trabecular bone mass may appear surprising. However, most of the aforementioned studies were centered on inflammation-related disease models (eg, rheumatoid arthritis, cancer) and focused largely on the ability of MIP family members to recruit immune cells under inflammatory conditions, whereas detailed in vivo studies examining the homeostatic role of these factors in bone formation and maintenance are lacking. Our data indicate that CCL20/CCR6 signaling may play an important role in fostering bone accrual, possibly by promoting osteoblast development and survival, representing a novel homeostatic function for this chemokine/receptor pair. These findings may not only apply to bone development and homeostasis but to fracture healing as well, suggesting further study in this area is warranted. Advantageously, the monogamous interaction between CCL20 and CCR6 makes the CCL20/CCR6 axis an attractive therapeutic target, increasing the translational potential of this line of investigation.

Disclosures

All authors state that they have no conflicts of interest.

Acknowledgments

Authors' roles: Study design: MD, KLW, and SLK. Study conduct: MD, SJ, ES, and BT. Data collection: MD, SJ, ES, and BT. Data analysis: MD, SJ, KLW, and SLK. Data interpretation: MD, KLW, and SLK. Drafting manuscript: MD and SLK. Revising manuscript content: MD and SLK. Approving final version of manuscript: MD, SJ, ES, BT, KLW, and SLK. SLK takes responsibility for the integrity of the data analysis.

References

1. Baba M, Imai T, Nishimura M, et al. Identification of CCR6, the specific receptor for a novel lymphocyte-directed CC chemokine LARC. J Biol Chem. 1997;272(23):14893–8.
2. Sallusto F, Lanzavecchia A. Understanding dendritic cell and T-lymphocyte traffic through the analysis of chemokine receptor expression. Immunol Rev. 2000;177:134–40.
3. Wang J, Adelson DL, Yilmaz A, Sze SH, Jin Y, Zhu JJ. Genomic organization, annotation, and ligand-receptor inferences of chicken chemokines and chemokine receptor genes based on comparative genomics. BMC Genomics. 2005;6:45.
4. Munoz I, Berges M, Bonsergent C, Cormier-Aline F, Quere P, Sibille P. Cloning, expression and functional characterization of chicken CCR6 and its ligand CCL20. Mol Immunol. 2009;47(2–3):551–9.
5. Krzysiek R, Lefevre EA, Bernard J, et al. Regulation of CCR6 chemokine receptor expression and responsiveness to macrophage inflammatory protein-3alpha/CCL20 in human B cells. Blood. 2000;96(7):2338–45.
6. Sisirak V, Vey N, Vanbervliet B, et al. CCR6/CCR10-mediated plasmacytoid dendritic cell recruitment to inflamed epithelia after instruction in lymphoid tissues. Blood. 2011;118(19):5130–40.
7. Yamazaki T, Yang XO, Chung Y, et al. CCR6 regulates the migration of inflammatory and regulatory T cells. J Immunol. 2008;181(12):8391–401.
8. Cook DN, Prosser DM, Forster R, et al. CCR6 mediates dendritic cell localization, lymphocyte homeostasis, and immune responses in mucosal tissue. Immunity. 2000;12(5):495–503.
9. Varona R, Villares R, Carramolino L, et al. CCR6-deficient mice have impaired leukocyte homeostasis and altered contact hypersensitivity and delayed-type hypersensitivity responses. J Clin Invest. 2001;107(6):R37–45.
10. Wen H, Hogaboam CM, Lukacs NW, Cook DN, Lira SA, Kunkel SL. The chemokine receptor CCR6 is an important component of the innate immune response. Eur J Immunol. 2007;37(9):2487–98.
11. Ghadjar P, Coupland SE, Na IK, et al. Chemokine receptor CCR6 expression level and liver metastases in colorectal cancer. J Clin Oncol. 2006;24(12):1910–6.
12. Marsigliante S, Vetrugno C, Muscella A. CCL20 induces migration and proliferation on breast epithelial cells. J Cell Physiol. 2013;228(9):1873–83.
13. Han JH, Choi SJ, Kurihara N, Koide M, Oba Y, Roodman GD. Macrophage inflammatory protein-1alpha is an osteoclastogenic factor in myeloma that is independent of receptor activator of nuclear factor kappaB ligand. Blood. 2001;97(11):3349–53.
14. Kominsky SL, Abdelmagid SM, Doucet M, Brady K, Weber KL. Macrophage inflammatory protein-1 delta: a novel osteoclast stimulating factor secreted by renal cell carcinoma bone metastasis. Cancer Res. 2008;68(5):1261–6.
15. Devoto M, Spotila LD, Stabley DL, et al. Univariate and bivariate variance component linkage analysis of a whole-genome scan for loci contributing to bone mineral density. Eur J Hum Genet. 2005;13(6):781–8.
16. Tang ZH, Xiao P, Lei SF, et al. A bivariate whole-genome linkage scan suggests several shared genomic regions for obesity and osteoporosis. J Clin Endocrinol Metab. 2007;92(7):2751–7.
17. Wilson SG, Reed PW, Andrew T, et al. A genome-screen of a large twin cohort reveals linkage for quantitative ultrasound of the calcaneus to 2q33-37 and 4q12-21. J Bone Miner Res. 2004;19(2):270–7.
18. Haudenschild DR, Nguyen B, Chen J, D'Lima DD, Lotz MK. Rho kinase-dependent CCL20 induced by dynamic compression of human chondrocytes. Arthritis Rheum. 2008;58(9):2735–42.
19. Lisignoli G, Manferdini C, Codeluppi K, et al. CCL20/CCR6 chemokine/receptor expression in bone tissue from osteoarthritis and rheumatoid arthritis patients: different response of osteoblasts in the two groups. J Cell Physiol. 2009;221(1):154–60.
20. Bouxsein ML, Boyd SK, Christiansen BA, Guldberg RE, Jepsen KJ, Muller R. Guidelines for assessment of bone microstructure in rodents using micro-computed tomography. J Bone Miner Res. 2010;25(7):1468–86.
21. Dempster DW, Compston JE, Drezner MK, et al. Standardized nomenclature, symbols, and units for bone histomorphometry: a 2012 update of the report of the ASBMR Histomorphometry Nomenclature Committee. J Bone Miner Res. 2013;28(1):2–17.
22. Al-Aoukaty A, Rolstad B, Giaid A, Maghazachi AA. MIP-3alpha, MIP-3beta and fractalkine induce the locomotion and the mobilization of intracellular calcium, and activate the heterotrimeric G proteins in human natural killer cells. Immunology. 1998;95(4):618–24.
23. Sanchez-Sanchez N, Riol-Blanco L, de la Rosa G, et al. Chemokine receptor CCR7 induces intracellular signaling that inhibits apoptosis of mature dendritic cells. Blood. 2004;104(3):619–25.
24. Ticchioni M, Essafi M, Jeandel PY, et al. Homeostatic chemokines increase survival of B-chronic lymphocytic leukemia cells through inactivation of transcription factor FOXO3a. Oncogene. 2007;26(50):7081–91.
25. Alexander KA, Chang MK, Maylin ER, et al. Osteal macrophages promote in vivo intramembranous bone healing in a mouse tibial injury model. J Bone Miner Res. 2011;26(7):1517–32.
26. Chang MK, Raggatt LJ, Alexander KA, et al. Osteal tissue macrophages are intercalated throughout human and mouse bone lining tissues and regulate osteoblast function in vitro and in vivo. J Immunol. 2008;181(2):1232–44.
27. Fernandes TJ, Hodge JM, Singh PP, et al. Cord blood-derived macrophage-lineage cells rapidly stimulate osteoblastic maturation in mesenchymal stem cells in a glycoprotein-130 dependent manner. PloS One. 2013;8(9):e73266.
28. Ahuja SS, Zhao S, Bellido T, Plotkin LI, Jimenez F, Bonewald LF. CD40 ligand blocks apoptosis induced by tumor necrosis factor alpha, glucocorticoids, and etoposide in osteoblasts and the osteocyte-like cell line murine long bone osteocyte-Y4. Endocrinology. 2003;144(5):1761–9.
29. Li Y, Toraldo G, Li A, et al. B cells and T cells are critical for the preservation of bone homeostasis and attainment of peak bone mass in vivo. Blood. 2007;109(9):3839–48.
30. Rifas L, Arackal S, Weitzmann MN. Inflammatory T cells rapidly induce differentiation of human bone marrow stromal cells into mature osteoblasts. J Cell Biochem. 2003;88(4):650–9.
31. Vi L, Baht GS, Whetstone H, et al. Macrophages promote osteoblastic differentiation in-vivo: implications in fracture repair and bone homeostasis. J Bone Miner Res. 2015;30(6):1090–102.
32. Lee AY, Phan TK, Hulett MD, Korner H. The relationship between CCR6 and its binding partners: does the CCR6-CCL20 axis have to be extended? Cytokine. 2015;72(1):97–101.
33. Gao Y, Wu X, Terauchi M, et al. T cells potentiate PTH-induced cortical bone loss through CD40L signaling. Cell Metab. 2008;8(2):132–45.